



J C M M

**Towards a similarity theory of
moist convective updrafts**

**Olaf Stiller
and
George C Craig**

May 2000

INTERNAL REPORT NO.115

NWP Technical Report No.310



Joint Centre for Mesoscale Meteorology

Towards a similarity theory of moist convective updrafts

By Olaf Stiller* and George C. Craig

University of Reading, UK

SUMMARY

The mixing of air between clouds and their environment is investigated with the help of a simplified model problem that contains only a small number of dynamically relevant parameters, whose influence can be systematically explored. The classical model of a buoyant thermal, extensively studied in laboratory experiments, is generalised to include the key moist processes of condensation and reevaporation of cloud water. We consider the evolution of an isolated thermal initiated from a spherical warm and moist bubble at rest in a moist neutral sounding. The moist thermal loses buoyancy through mixing with the unsaturated environmental air, and finally collapses. The effect of moist physics on the thermal is shown to be represented by only three scale-independent parameters. As is expected for real clouds, these thermals do depend on their initial conditions, and therefore are *not self-similar*. However, we present large eddy simulations that exhibit an approximate *dynamical similarity*, in that the loss of buoyancy resulting from the mixing process is mainly described by a single scale-invariant parameter which we call the effective buoyancy, B_{eff} . In order for the thermal to ascend a distance significantly larger than its initial diameter, B_{eff} must be much greater than unity. This implies that the environment must be close to saturation if the bubble has an initial buoyancy that is typical of real clouds. It is also shown that the stratification of the environment induces a length scale, L_{buo} , for a thermal with a given buoyancy excess. The resulting scale-independent parameter $L_{eff} = L/L_{buo}$ (where L is the initial bubble radius) is shown to affect the geometry of the thermal. Indeed, the thermal may break up if L_{eff} is too large. These geometrical effects can be explained by relating L_{buo} to the depth reached by forced downdrafts, which corresponds to the vertical extent of the largest eddies that entrain unsaturated air into the thermal.

KEYWORDS: convection thermal similarity theory

1. INTRODUCTION

One of the most important unsolved problems of cumulus convection is that of mixing of the buoyant cloudy air with the dry air of the cloud's environment. This mixing leads to re-evaporation of cloud water, reducing the buoyancy of the cloudy air, and altering the microphysical processes that determine the fate of the hydrometers within the cloud. The bulk properties of the convective cloud, that must be ascertained to determine its effects on larger scales of motion in the atmosphere, are also strongly affected by mixing. These properties include the cloud top height, and indeed the entire vertical profile of mass transport by the cloud, as well as the precipitation and the vertical transport of moisture and heat.

Early theories of convective mixing were based on an assumption of self-similarity, where the mixing was a result of a fully-developed turbulent field with no intrinsic length or time scales, apart from those provided by the constraints of the initial volume of buoyant air (Morton et al. 1956). These ideas were tested against laboratory experiments in which buoyant fluid was introduced into a neutrally stratified environment. Two experimental configurations have been widely employed (e.g. Morton 1997). The first is the *thermal*, where a discrete bubble with a known volume of buoyant fluid is released suddenly at the initial time. The second is the *plume*, where a continuous stream of buoyant fluid is released from a pipe, giving a known buoyancy flux. In each case the size of the initial bubble or pipe is designed to be small in comparison to the eventual size of the thermal or plume. When the fluid has moved a sufficient distance from the source, the turbulence has developed to the point where the initial conditions at the source are

* Corresponding author: Department of Meteorology, University of Reading, 2 Earley Gate, Whiteknights, Reading, Berkshire, RG6 6BB, UK.

forgotten. Environmental fluid is then entrained at a constant rate, leading to a linear increase in size of the thermal or plume with distance from the source, but no change in shape or structure. In other words, the flow is *self-similar*. The linear spread is the natural result of the absence of any intrinsic length scales in the experiment, other than the distance from the source.

Self-similarity in these problems is equivalent to the *entrainment hypothesis* introduced by Morton et al. (1956), and discussed further by Turner (1986). It is hypothesised that the rate of entrainment of environmental fluid is determined by the local vertical velocity averaged over the rising fluid within the thermal or plume. The entrainment hypothesis appears to work well even in situations where self-similarity does not occur. A prime example is the injection of a thermal or plume into a stably stratified fluid. In this problem the entity may spread linearly for some time, but eventually the self-similar structure breaks down, on a length scale proportional to the level of zero buoyancy of the injected fluid in the absence of mixing. As it loses buoyancy, the injected fluid spreads horizontally. The level at which this spreading occurs is accurately predicted by the entrainment hypothesis (Turner 1973), although the reasons for its success remain obscure (Morton 1997). Presumably, at any given level, the turbulence must have a self-similar structure. This appears reasonable in the experiments discussed above, where the distance from the source to the level of zero buoyancy is large compared to the dimensions of the initial source (which must be forgotten). However, the constant of proportionality between the entrainment rate and mean vertical velocity (the *entrainment constant*) depends on the experimental configuration and is different for thermals and plumes.

The success of the entrainment hypothesis for laboratory flows prompted its application to cumulus convection in the atmosphere (Ludlam and Scorer 1953, Malkus and Scorer 1955). A moisture conservation equation was added to the dynamical equations, and mixing was parameterised using an entrainment constant obtained from the experiments on idealised laboratory flows (Morton 1956, Squires and Turner 1962). The further progress of these attempts is reviewed by Turner (1973), Blyth (1993), and Bretherton (1997) and will not be discussed in detail here, except to quote the conclusion of Turner (1973): "In retrospect, it seems clear that clouds (which are typically nearly as broad as they are tall) will not achieve a fully developed state, and are poor candidates for the application of similarity theories which describe the steady flow many diameters above a small source." The failure of cumulus clouds to reach a fully developed, self-similar state is apparent in the observation that some subcloud air is often observed to reach the cloud top level without significant dilution, while observations of liquid water content show that most of the cloud air has been significantly diluted (Warner 1970). If the entrainment parameter in a thermal or plume model of a cloud is chosen to be large, the cloud air will be strongly diluted and will lose buoyancy rapidly. The cloud top height will then be underpredicted. If the entrainment rate is chosen to be small enough to predict a reasonable cloud top height, too little mixing and re-evaporation will occur and the liquid water content will be overestimated.

Recent research has studied the inhomogeneous structures in clouds, including bubbles of buoyant air and penetrative downdraughts that are often observed (Blyth 1993, Bretherton 1997). The study of these structures has prompted the development of mixing models based on discrete entities, upward and downward moving parcels of air that mix in various proportions with their environments. However, these theories lack the rigorous theoretical basis of the earlier entrainment models and contain many *ad hoc* parameters relating to number and properties of entities, proportions of mixing, and precipitation efficiency. In the absence of firm understanding of the mixing process, it is perhaps not surprising that the entrainment hypothesis, with all its flaws, is still often employed in

cumulus parameterisation schemes (e.g. Arakawa and Schubert 1974, Tiedtke 1989, Kain and Fritsch 1990).

While the failure of the entrainment hypothesis is consistent with a breakdown of self-similarity on the scale of the cloud itself, there is some evidence that fully developed turbulence exists on smaller scales within clouds. Fine-scale aircraft and balloon observations of small convective clouds show power-law scaling of the vertical velocity variance, which would be expected in a self-similar turbulent cascade (Kitchen and Caughey 1981, Smith and Jonas 1995). While these authors found that there is sometimes a suggestion of a peak at small (10-20 m) scales, there is no compelling evidence of a significant input of energy on scales much smaller than the cloud itself. However, because of the small number of clouds sampled, the results have little statistical significance at the largest scales. Baker (1992) finds evidence of inhomogeneity in droplet concentrations on scales of 5-10 cm, but homogeneity on larger scales up to the cloud turret size of 100-1000 m. It has also been suggested, on the basis of two-dimensional numerical experiments (Klaassen and Clark 1985), that there is an instability that might take place on cloud boundaries, introducing energy on a preferred scale that is smaller than the cloud itself, but it is difficult to determine what that scale should be. The growth of a cumulus cloud as a number of bubbles or turrets is sometimes observed (French et al. 1999), but not always (Barnes et al. 1996). This might be due to multiple releases of buoyant air from the boundary layer, or might result from an instability of a single initial burst. It remains an open question whether there is an intrinsic scale that determines the size of the entities involved in mixing, other than the scale of the cloud itself.

Abandoning temporarily the goal of understanding the entire cumulus cloud, a number of studies have explored the mixing process in idealised flows that capture certain aspects of the convective problem. It is difficult to examine the near-field behaviour of a thermal in the laboratory, because of the difficulty of precisely reproducing the initial conditions on which the behaviour now depends. This problem was addressed by Sánchez et al. (1989), who devised a method for releasing bubbles of buoyant fluid from a motionless initial state. The resulting thermals exhibited a reproducible vortex ring structure, resulting in a smaller entrainment rate than found for fully-developed turbulence. To examine the effects of latent heat release on mixing, Venkatakrisnan et al. (1999) have studied the effect on a buoyant plume of electrically heating the plume fluid. They found that the heating disrupted the turbulent structures and reduced the rate of mixing in the plume, although the mass flux was not greatly changed, since the velocity of the plume accelerated. Johari (1992), following the pioneering work of Turner and Yang (1963), considered the effects of the buoyancy reversal that occurs when re-evaporating liquid water cools the buoyant air. Buoyant thermals were released, using an alcohol-water mixture that became negatively buoyant when mixed with the environmental fluid. Surprisingly, it was found that the small-scale mixing seemed largely unaffected by buoyancy reversal, even though the trajectory of the thermal was quite different. Baker and Breidenthal (1984) examined the turbulent structure on microscopic scales, applying a model based on chemically reacting shear layers, in order to explain the microphysical variability in clouds. While each of these studies captures important aspects of a convective cloud, the authors have prudently limited themselves to systems that can be reproduced in the laboratory, giving confidence that the results are correct, although the applicability to the atmosphere requires further investigation.

A more speculative approach to the study of convective mixing involves the use of numerical models as proxies for unobtainable laboratory or observational data. Most practical simulations depend on the large eddy modelling hypothesis (Mason 1994): that it is sufficient to explicitly model the large, energy-containing eddies in a turbulent flow.

It is hoped that the smaller eddies will be controlled by a turbulent cascade from the larger scales, and the bulk behaviour of the fluid will be independent of the details of the small-scale flow. This assumption has proved useful in simulating a great variety of turbulent flows (e.g. Lesieur 1997). Circumstantial support for the application to cloud modelling is provided by observational studies that indicate a homogeneous turbulent structure on scales from 1-100 m (Smith and Jonas 1995, Baker 1992). Indeed recent simulations of shallow cumuli using 50 m resolution (Carpenter et al. 1998) show a remarkable qualitative resemblance to real clouds. One advantage of numerical models is that the physics of the model can be modified and simplified to gain insight into the effects of individual physical processes. This approach was taken by Grabowski (1993, 1995) who carried out an elegant series of numerical experiments that demonstrated the role of buoyancy reversal in creating inhomogeneous structures in the simulated clouds. Importantly the simulations agreed with the laboratory experiments of Johari (1992) in showing that buoyancy reversal had little effect on the rate of fine-scale mixing between the cloud and environment. It is clear that numerical models offer a powerful tool for the study of entrainment and mixing in convective clouds, but it must be acknowledged that the parameterisations of subgrid mixing are largely untested where phase changes of water are involved, and the results can only be regarded as hypotheses for testing in the laboratory and in the outside world.

The investigation described in this paper is a preliminary attempt to address some of the key questions of mixing in convective clouds. In the absence of a simple self-symmetry, it is important to identify what scales of motion are present in the problem, and how they are produced. To this end, we present a systematic analysis of a model problem that includes the effects of latent heat release, buoyancy reversal due to re-evaporation, and a simple removal of precipitation that ignores most of the complexity associated with cloud microphysics. The problem chosen is a generalisation of the classical buoyant thermal, namely a spherical bubble of saturated air released from rest into an unsaturated atmosphere that is stratified at the moist adiabatic lapse rate. Because both latent heat release and buoyancy reversal are included, this is a more realistic system than available laboratory analogues. We test our theoretical understanding against numerical simulations using a large eddy model. Unfortunately this gives us less confidence in our results than can be obtained in the laboratory, due to the parameterisations employed in the model.

It should be emphasised that this is a study of the mixing process, rather than an attempt to simulate a realistic cloud. As discussed in the conclusions, it is possible to relate certain aspects of the simulations to the behaviour of entities such as bubbles or turrets within clouds, but the extent of this analogy is limited. What we hope to show is that the model problem can be characterised by a small number of parameters, including characteristic length and time scales. These will correspond to a small number of *nondimensional* parameters and the thermal will then exhibit *dynamical similarity*, i.e. different realisations of the flow with very different dimensional parameter values evolve in a similar way, provided that they share the same values of the nondimensional parameters. This dynamical similarity is a much weaker result than the self-similarity of the classical thermal in the far field, where the structure of the thermal at any given time is similar to itself at all other times. However, it is still an important result, if it can be shown that some of the nondimensional parameters are more important than others in controlling the evolution of the flow. The dominant parameter, or parameters, will correspond to the essential physical processes involved in the flow, allowing their role to be unambiguously and quantitatively identified.

2. THE SIMPLIFIED MODEL EQUATIONS

We take as a starting point the anelastic equations of motion for momentum and for conserved, linearly mixing scalar variables Ψ

$$\frac{D}{Dt} u_i = -\partial_{x_i} \left[\frac{p'}{\rho_s} \right] + \delta_{i3} B + \rho_s^{-1} \partial_{x_j} [\rho_s \nu S_{ij}] \quad (1)$$

$$\frac{D}{Dt} \Psi = -\partial_{x_i} [\rho_s \nu \partial_{x_i} \Psi] \quad (2)$$

where Einstein's summation convention of summation over any index repeated once (in a product or similar expression) has been used. The partial derivative with respect to the space variable x_i is written as ∂_{x_i} . Similarly we use ∂_t for the partial time derivative so that the total time derivative of a fluid parcel can be written as

$$\frac{D}{Dt} = \partial_t + u_i \partial_{x_i} \quad (3)$$

The theoretical conclusions developed in this paper will be tested against numerical simulations using a large-eddy model that uses a first order closure to represent unresolved turbulent motions. The turbulence parameterisation introduces a Richardson number dependent eddy viscosity ν , as seen in the last terms on the rhs of Eqs. (1,2) where $S_{ij} = \partial_{x_i} u_j + \partial_{x_j} u_i$. The details of the parameterisation are given by Shutts and Gray (1994). Formally this closure introduces, as part of ν , a scale-dependent parameter λ , the subgrid mixing length. However, in this work, it is assumed that subgrid turbulence has lost its scale dependence and thus the results should be essentially independent of λ . This assumption is also the justification for the use of large-eddy model (Mason 1994), and is therefore not tested when the theory is compared to simulations.

As usual p' in Eq. (1) is the pressure difference from the reference pressure p_s of the environment which is in hydrostatic balance. In this article profiles of the environmental sounding are generally referred to by the subscript s (e.g. ρ_s , θ_s or T_s for density, potential temperature and temperature). Equation (1) results from a linearisation in pressure and potential temperature around the reference profiles which yields for the buoyancy force (water loading effects are neglected)

$$B = g \frac{\Delta\theta}{\theta_s} \approx g \frac{\Delta T}{T_s} \quad (4)$$

where g is the gravitational acceleration, $\Delta\theta = \theta - \theta_s$ and $\Delta T = T - T_s$. In the last step we used the definition of potential temperature with $p \approx p_s$ which neglects temperature dependence of the pressure as well as the dynamic pressure.

The thermodynamic scalars (Ψ in Eq. (2)) used in our numerical model are the total water mixing ratio q_t and moist static energy h with

$$h = c_p T + gz + L_v q_v \quad (5)$$

where c_p and L_v are the heat capacity of air at constant pressure and the latent heat of vapourisation. Both are assumed to be constant. The temperature is denoted by T , while q_v is the water vapour mixing ratio. The total water mixing ratio q_t is governed by Eq. (2) with the restriction that water is taken out irreversibly from the system if $q_t = \max(q_t - q_{sat}, 0)$ surpasses a threshold value $q_{t,max}$, where q_{sat} is the saturation mixing ratio. The value of $q_{t,max}$ can be chosen independently and serves to investigate the impact of the cloud water content on the mixing process. The buoyancy variable

ΔT (see Eq. 4) is most conveniently expressed in terms of deviations from the reference profiles, namely the *water vapour deficit* $q_{def} = q_{sat} - q_v$, and *moist static energy excess* $\Delta h = h - h_s^*$ which is the difference of h from its environmental saturation value $h_s^* = c_p T_s + gz + L_v q_{sat}$. One has

$$\Delta h = c_p \Delta T - L_v q_{def} \quad (6)$$

$$\text{or } B = g \frac{\Delta h + L_v q_{def}}{c_p T_s} \quad (7)$$

The saturation value of water vapour q_{sat} is assumed to be a linear function of height in our simplified model. We write

$$\frac{d}{dz} q_{sat} = -s_q \quad (8)$$

where s_q is a positive constant. Using this, the equation of motion for Δh can be written as

$$\frac{D}{Dt} \Delta h = (-c_p \Delta \Gamma + L_v s_q) w + \text{diffusive mixing} \quad (9)$$

where

$$\Delta \Gamma = \frac{dT_s}{dz} + \frac{g}{c_p} \quad (10)$$

is the difference of the lapse rate from that of a dry adiabatic sounding. Turbulent diffusive mixing is clearly essential for the loss of buoyancy of a parcel of air, but since it is assumed that subgrid turbulence has lost its scale dependence, no scale-dependent parameter is introduced by the last term in Eq. (9).

In the next subsection we discuss how mixing affects the thermodynamic properties of a parcel. As mentioned in the introduction, we will restrict attention to the case of a moist neutral environment. For such a moist adiabat Δh is conserved under adiabatic motion since $h_s^* = \text{const.}$ The lapse rate is then determined by the saturation curve (or vice versa):

$$\Delta \Gamma = -\frac{L_v}{c_p} \frac{dq_{sat}}{dz} \quad (11)$$

so that the first term on the rhs in Eq. (9) vanishes, and the buoyancy of a saturated parcel will only be changed by mixing (and the slow variations of $T_s^{-1}(z)$ in Eq. 7).

(a) Properties of mixed air

Figure 1 shows the effect the mixing process has on the thermodynamic properties of cloudy air. The degree of mixing is labeled by the fraction α of environmental air in the mixture. One of the most important properties of the air parcel is the moist static energy excess, Δh , of a mixture (grey solid line in Fig. 1, I, II). If the environmental sounding is a moist adiabat (as for the experiments presented in this article), Δh largely determines the the long-term destiny of a mixed parcel. Only parcels with $\Delta h > 0$ may rise with the cloud for long distances. If parcels with $\Delta h < 0$ happen to be positively buoyant they are according to Eq. (7) unsaturated, (i.e. $q_{def} > 0$), and therefore lose their buoyancy as they rise. The value of Δh for undilute cloud air is denoted Δh_{cloud} . Since Δh is the difference between the moist static energy of the parcel and the saturation value at

the environmental temperature, its value for undilute environment air is $-L_v q_{def}$. The mixing curve of Δh is a straight line and the value α_{crit} where this line crosses the α axis is determined by $\Delta h_{cloud}/L_v q_{def}$, the ratio of Δh at $\alpha = 0$ and $\alpha = 1$. One has

$$\frac{\alpha_{crit}}{1 - \alpha_{crit}} = \frac{\Delta h_{cloud}}{L_v q_{def}} = \frac{c_p \Delta T_{cloud}}{L_v q_{def}} = B_{eff} . \quad (12)$$

(One way to see this is by noting that the two triangles formed when the Δh line and the α axis cross the two vertical lines at $\alpha = 0$ and $\alpha = 1$ are geometrically similar so that the ratios of all corresponding sides have the same value.) In the last step of Eq.(12) we have introduced a dimensionless parameter which we call *effective buoyancy* $B_{eff} = c_p \Delta T_{cloud}/(L_v q_{def})$. According to Eq. (12) B_{eff} gives the ratio of the range of α values with $\Delta h > 0$ divided by that with $\Delta h < 0$. It is a measure for the heat excess of the updraft compared to the reevaporative cooling that can result from mixing with environmental air.

The dark solid lines in Fig. 1 Ia,b are $c_p \Delta T$, which according to Eq.(4) is a direct measure of buoyancy. For large values of α , where the parcel is saturated, $c_p \Delta T$ is identical to Δh . Once sufficient environmental air has been mixed into the parcel to evaporate all the liquid water, $c_p \Delta T$ leaves the Δh line and mixes linearly to the environmental value $\Delta T = 0$ at $\alpha = 1$. The value α_{max} at which the "buoyancy curve" leaves the " Δh line" is entirely determined by the ratio q_l/q_{def} . One finds

$$\frac{\alpha_{max}}{1 - \alpha_{max}} = \frac{q_l}{q_{def}} . \quad (13)$$

To see this it is convenient to consider the Δh_l line (dotted line in Fig. 1, I,II). $\Delta h_l = h_l - h_{l,s}$ is the difference of the liquid water static energy $h_l = c_p T + gz - L_v q_l$ from its environmental value $h_{l,s} = c_p T_s + gz$. In the unsaturated case $c_p \Delta T$ is identical to $\Delta h_l = c_p \Delta T - L_v q_l$ and α_{max} is therefore given by the intersection of the Δh with the Δh_l line. The first equality in Eq. (13) follows from the similarity of the triangles which are formed by the Δh and the Δh_l lines with the vertical axes at $\alpha = 0$ and $\alpha = 1$.

Buoyancy reversal through mixing requires that the cloud water content q_l is large enough to compensate the cloud's buoyancy excess, i.e. $L_v q_l > \Delta h_{cloud}$. Figure 1 Ib gives an example where q_l is too small, so that all mixtures are positively buoyant. But dry parcels lose buoyancy as they rise, and the conservation of $\Delta h = \Delta T - L_v q_{def}$ directly implies that only those mixtures with $\alpha < \alpha_{crit}$ remain buoyant when lifted to their condensation level. Consequently α_{crit} is expected to be more important than α_{max} , and thus q_{def} should play a more crucial role than q_l for the cloud's loss of buoyancy through mixing.

The liquid cloud water has, however, a strong influence on the level at which mixtures that leave the cloud (i.e. those with $\Delta h < 0$) become neutrally buoyant. As shown below, the distance L_{down} which a detrained parcel descends from the level z_0 to its level of neutral buoyancy z_{lnb} is given by *

$$L_{down} = z_0 - z_{lnb} = -\frac{1}{L_v s_q} \Delta h_l . \quad (14)$$

The fact that the downdraft length is proportional to Δh_l for $\alpha > \alpha_{crit}$ is illustrated by the dark solid line in Fig. 1 II. For a positively buoyant cloud L_{down} is always smaller than

* The name L_{down} should not obscure the fact that Eq. 14 actually also holds for $L_v q_l < c_p \Delta T$ (as in Fig. 1 Ib) for which L_{down} becomes negative (i.e. the z_{lnb} is above z_0). The only assumption in deriving Eq. (14) is that $q_l = 0$ at z_{lnb} which is identical to $\alpha > \alpha_{crit}$.

the downdraft length $L_{dmax} = q_l/s_q$ of a neutrally buoyant parcel for which $\Delta h_l = -L_v q_l$. (The expression $L_{dmax} = L_v q_{lmax}/c_p \Delta \Gamma$ used in table 2 is obtained by applying the above definition to the case $q_l = q_{lmax}$ and using $s_q = c_p \Delta \Gamma/L_v$ - see Eq. 11.)

Equation (14) is obtained by noting that Δh_l is related to Δh by $\Delta h_l = \Delta h - L_v(q_t - q_{sat})$ so that (adiabatic) changes of Δh_l are entirely determined by changes of the saturation curve, i.e.

$$\Delta h_l(z) = \Delta h_l(z_0) + L_v (q_{sat}(z) - q_{sat}(z_0)) . \quad (15)$$

The level of neutral buoyancy is characterised by both $\Delta T = 0$ and $q_l = 0$, since the case where $\Delta T = 0$ and $q_l \neq 0$ is unstable to small perturbations in ΔT . Therefore $\Delta h_l = c_p \Delta T - L_v q_l = 0$ is a necessary condition, which together with $q_{sat}(z_{lnb}) - q_{sat}(z_0) = s_q(z_0 - z_{lnb})$ (see Eq. 8) leads to Eq. (14). By using the criterion $\Delta h_l = 0$ we assume that a level of neutral buoyancy with $q_l = 0$ would exist. This is of course only true if the parcel actually is detrained or equivalently $\alpha > \alpha_{crit}$ (see discussion above).

3. THE EXPERIMENTAL SET UP

In the experiments discussed in this article we have initialised a warm and moist (i.e. saturated) bubble in a sounding which is neutral to moist adiabatic ascent. The bubble we are considering in this first study has the form of a sphere with a radius L and constant buoyancy. In the numerical simulations, the buoyancy is decreased linearly to the environmental value in a shell of thickness $L/6$ to avoid extreme temperature gradients. To characterise the initial buoyancy excess of the bubble we will use ΔT^0 which is the initial temperature excess in the middle of the bubble.

A further key parameter is the water vapour deficit $q_{def} = q_{sat} - q_v$ of the surrounding air (environment), which in our experiments has an uniform initial value of q_{def}^0 . If no mixing occurred, Δh would be conserved and the buoyant air would remain buoyant and rise forever. If the environment were saturated, the mixing process would not affect the total buoyancy flux which would remain positive and vary only very slowly as a function of height. The loss of buoyancy (or moist static energy), which finally stops the rising motion, results from the water vapour deficit of the surrounding air that mixes with the saturated bubble air.

Table 1 lists the parameters in our system which can be used to label each experiment. Parameters are listed according to whether they are related to the initial conditions of bubble and environment or whether they are part of the "model physics". Note that some of these parameters are not independent for the particular choice of experiments conducted in this study. The horizontal and vertical length scales are the same, i.e. $L = H$, for the spherical bubble used in all the simulations presented here. Furthermore, since the environmental sounding is a moist adiabat, its lapse rate is determined by the gradient of the saturation curve (or vice versa), yielding $\Delta \Gamma = \frac{L_v}{c_p} s_q$ (Eq. 11).

(a) Scale independent parameters

The model has been designed to minimise the number of parameters while representing some essential features of moist convection. This subsection is devoted to the enumeration of the *scale-independent* parameters occurring in this system. Since the physics may not depend on the units we are using to measure it, it is clear that only these scale-independent parameters can determine the behaviour of the bubble. The simple dry thermals (investigated in earlier studies) could successfully be described with the help of similarity theory since they depended upon only a very small number of scale-independent

parameters. The moist bubbles considered here have some additional parameters related to moisture which makes a scaling hypothesis less straight forward. The principle questions we ask in this article are; which are the scale-independent parameters in this system and in what way does the mixing process and the dynamics of the bubble depend on them?

A complete set of scale-independent parameters may be constructed by taking products of the scale-dependent parameters listed in Table 1. Let us first note that the mixing ratios of different water substances, q_{def}^0 , q_{lmax} and q_{sat} , enter the equations of motion only through the corresponding latent heat, $L_v q_{def}^0$, $L_v q_{lmax}$ and $L_v q_{sat}$. Therefore, even though mixing ratios are dimensionless, they are not scale-independent parameters that are relevant for the dynamics of the system. Table 2 lists a complete set of scale-independent parameters constructed from the parameters in Table 1. This set of parameters is not uniquely defined; for example, either a relative downdraft depth or an effective negative buoyancy could be employed. However, the number of independent parameters is uniquely determined. Note that we do not investigate the influence of any purely geometrical parameter, such as the aspect ratio of the initial bubble, as the current study is restricted to spherical bubbles. Thus we are left with three moisture-related scale-independent parameters to label our numerical experiments. The physical significance of these parameters will be discussed in detail below.

TABLE 1. MODEL PARAMETERS

environment		bubble		physics	
lapse rate diff. (dry stability)	$\Delta\Gamma$	temperature excess	ΔT^0	maximal cloud water	q_{lmax}
water vapour deficit	q_{def}^0	geometry: Length, Height, etc.	$L, H,$ etc.	gradient of saturation curve	$\frac{\partial}{\partial z} q_{sat}$

Table 1: List of parameters in the system. Parameters are divided into three groups, depending on whether they result from the initial conditions of the environment, of the bubble, or from the "model physics".

TABLE 2. SCALE-INDEPENDENT MODEL PARAMETERS.

1)	effective buoyancy excess	$B_{eff} = \frac{c_p \Delta T^0}{L_v q_{def}}$
2)	effective bubble size (buoyancy length scale:)	$L_{eff} = \frac{L}{L_{buo}}$ ($L_{buo} = \frac{\Delta T^0}{\Delta\Gamma}$)
3)	relative downdraft depth (maximum downdraft depth) alternatively: effective negative buoyancy	$L_{dmax} = \frac{L_{dmax}}{c_p \Delta\Gamma}$ $\frac{L_v q_{lmax}}{c_p \Delta T^0} = \frac{L_{dmax}}{L_{buo}}$
geometry related:		
aspect ratio, etc.		$\frac{L}{H},$ etc.

(b) The dominant time scale

A good order of magnitude estimate for a scale dependent quantity can often be obtained by using the appropriate scales which are dominant for the quantity's evolution. To obtain the dominant time scale we look at the equations of motion and neglect the effect of mixing. Then, for a moist rising bubble, $\Delta h = c_p \Delta T$ is conserved at its initial value $c_p \Delta T^0$. Assuming further that the bubble radius L is the only relevant length scale,

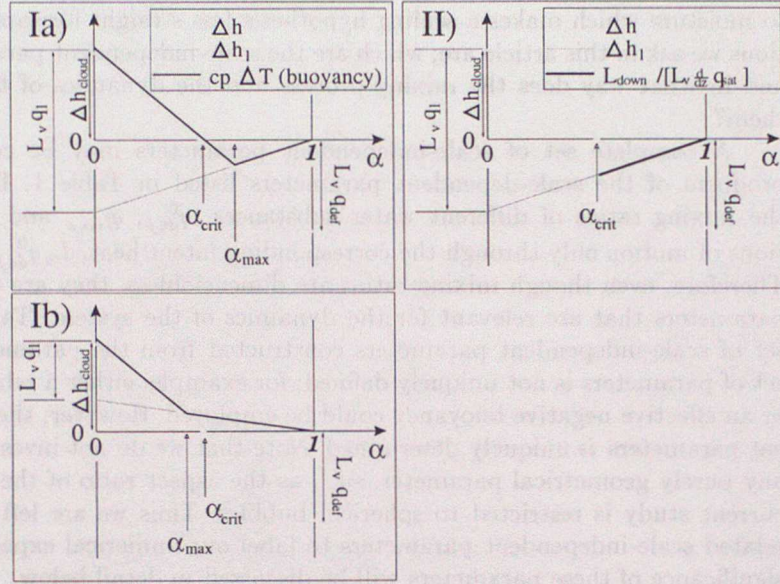


Figure 1. Mixing diagrams for moist static energy excess Δh (grey solid line) and liquid water static energy excess Δh_l (dotted line) as function of the fraction of entrained environmental air α . In figures Ia) and Ib) the dark solid line indicates $c_p \Delta T$ (a more direct measure for buoyancy). In figure II) the dark solid line is proportional to the downdraft length L_{down} .

the momentum equation

$$\frac{D}{Dt} u_i = -\partial_{x_i} \left[\frac{p'}{\rho_s} \right] + \delta_{i3} g \frac{\Delta T^0}{T_s} \quad (16)$$

posses only one time scale

$$T_{buo} = \sqrt{\frac{L T_s}{g \Delta T^0}} \propto \sqrt{\frac{L}{\Delta T^0}} \quad (17)$$

where we choose a fixed reference value of T_s . For dry air ΔT is not conserved (even in the absence of mixing) and a similar analysis yields the Brunt-Väisälä time scale T_{BV} (the inverse of the Brunt-Väisälä frequency) which is obtained by replacing $\frac{L}{\Delta T^0}$ by $(\Delta \Gamma)^{-1}$ in Eq. (17). The Brunt-Väisälä time scale is the scale at which the environment tries to restore the stratification (which is perturbed by the rising bubble) while T_{buo} is the time scale responsible for the bubble's ascent. Note that the effective bubble size $L_{eff} = \frac{L \Delta \Gamma}{\Delta T^0}$ can (alternatively) be written as the ratio of the two time scales, $L_{eff} = [T_{buo}/T_{BV}]^2$. For the evolution of the bubble T_{buo} is the dominant time scale and when comparing data from different runs in the next section all scale-dependent variables will be nondimensionalised using the following scales: T_{buo} for time, L for space and ΔT^0 for temperature ($\frac{L}{T_{buo}}$ for velocity, etc.). This has the advantage that data from different runs with different orders of magnitude of temperature, humidity (given by q_{def}), etc. assume the same order of magnitude, so that the effects of the scale independent parameters (which by definition can not be scaled away) become visible.

4. RESULTS OF SIMULATIONS

In this section we present results from nine numerical experiments with parameter values listed in Table 3. The initial bubble radius in all experiments is $L = 720$ meters, and the effective down draft length L_{dmax} is kept constant at a value of $L_{dmax} = 0.52$, which corresponds to $q_{lmax} = 0.75g/kg$. The effect which changes in L_{dmax} have on the bubble dynamics will be investigated in a future study.

Quantitative simulation data will be presented in two different ways: (a) as time series and (b) as (time and area integrated) fluxes plotted against physical height. While the time series illustrate the temporal evolution of the updraft, the flux/height plots show the effect of the bubble on the atmosphere, integrated over its lifetime. All the data will be scaled in the manner discussed in section 3. It will be seen that this indeed turns out to be the appropriate scaling, as data which would differ in their order of magnitudes when viewed in their "original scales" are of comparable magnitude when rescaled. This allows the control of the mixing process by the scale-independent parameters introduced in section 3 to be clearly identified. It will be seen that B_{eff} is indeed the dominant parameter determining the effect of the mixing on the bubble, as suggested by our theoretical considerations above. Further we offer a physical interpretation for the buoyancy length L_{buo} (see table 2) which yields an upper limit for the size of the entraining eddies, with interesting consequences for the geometry of the cloud.

(a) *The time evolution of the updraft*

Snapshots of a bubble as it develops from the initial simple sphere to a finer structure are given in Fig. 2. Plotted is Δh (left panels), which illustrates the buoyancy distribution, and cloud water (right panels), which gives an impression of the visual appearance of the cloud. From the Δh graphs entrainment is seen to erode the buoyancy in the middle of the updraft while the most buoyant air remains in a vortex ring structure which drifts apart as the cloud rises and fades away. At $t = 4.7$ the cloud liquid water shows a mushroom shape, whereas at $t = 9.4$ it has developed a much finer structure somewhat closer to the familiar cauliflower shape of real clouds.

For a more quantitative description, the temporal evolution of some quantities is given in Fig. 3, where different line thicknesses correspond to different (initial) values of B_{eff} . The dimensional values of initial buoyancy in these runs varies by more than an order of magnitude (Table 3). The similar magnitudes of the different curves demonstrates that the chosen time, space and temperature scales are appropriate.

As seen from the top graph, the maximal vertical velocity w_{max} exhibits an almost constant acceleration during the first time unit. Here bubbles with the same initial buoyancy, and hence the same L_{eff} , fall on the same curve indicating that they are not affected by mixing at this stage. Correspondingly, at the time of the earliest snapshot ($t = 1.2$) in Fig. 2, the bubble retains a smooth ellipsoidal shape. The fact that the more buoyant bubbles (larger ΔT^0 implying smaller L_{eff}) initially accelerate slightly faster than the weaker ones (see w_{max} in Fig. 3) may be attributed to the stratification of the environment. This is apparent since L_{eff} can also be interpreted as $L_{eff} = [T_{buo}/T_{BV}]^2$, that is, as the square of the ratio of the time scale of the moist bubble ascent to the Brunt-Väisälä time scale T_{BV} of the stratified environment. At approximately $t = 1.3$, w_{max} has a relatively sharp peak, after which it decreases and begins to fluctuate strongly. At the same time, the curves with the same buoyancy, but different q_{def} and thus B_{eff} , begin to separate, showing the first influence of the mixing process. Correspondingly, the first signs of entrainment of air from below are also visible in the second snapshot at $t = 2.4$ in Fig. 2.

The second plot in Fig. 3 shows T_{max} , the maximum of ΔT within the "active

cloud" (defined as the region where $\Delta h > 0$). As with w_{max} the scaled values of T_{max} are similar at first, but at about $t = 2.5$ they separate and begin to decrease. Again similarly to w_{max} , the curves fluctuate considerably once mixing has started to influence their evolution.

In contrast to this, fluctuations appear to be less chaotic for the volume-integrated quantities shown in the lower two graphs of Fig. 3, which illustrate the loss of buoyancy of the updraft more systematically. The decay of the bubble is seen to depend most sensitively on the effective buoyancy B_{eff} , and varies relatively weakly with the actual buoyancy. The volume of the active cloud, shown in the third plot of Fig. 3, increases when B_{eff} is sufficiently large, stays roughly constant when B_{eff} is of order unity, and decreases for B_{eff} small. This is in good qualitative agreement with the mixing diagrams discussed in section 2, where it was shown that $B_{eff} = \alpha_{crit}/(1 - \alpha_{crit})$, implying that B_{eff} is the ratio of the range of mixtures that are "actively buoyant" (i.e. $\Delta h > 0$) to those that are nonbuoyant when lifted to their condensation level. Of course the effective buoyancy decreases with time (the indicated value of B_{eff} in Fig. 3 corresponds only to the initial conditions) and the volume of buoyant air in all updrafts eventually decreases to zero. This steady decrease of buoyancy is clearly seen in the bottom graph of Fig. 3 which shows the (density weighted) integral of Δh over the active cloud where $\Delta h > 0$.

TABLE 3.

$\Delta T^0/[K]$	$q_{def}/[g/kg]$	B_{eff}	L_{eff}
4.3	0.55	3.15	0.83
	1.24	1.4	
	2.48	0.7	
0.48	0.061	3.15	7.5
	0.138	1.4	
	0.275	0.7	
0.12	0.015	3.15	30
	0.034	1.4	
	0.069	0.7	

Parameters of runs corresponding to the data in Figs. 3 and 4

(b) The spatial structure of vertical fluxes

In Figure 4 we show the height dependence of vertical fluxes which are integrated over time and over the horizontal area of the system. The plotted data correspond to the same runs as in the time series in Fig. 3, and use the same line styles. As with the time series in the last section, it is seen from Fig. 4 that B_{eff} is also the dominant parameter with respect to the time-integrated vertical fluxes. Although the actual buoyancy, and hence L_{eff} varies by a factor of 36 among the simulations, the fluxes depend more on the much smaller changes in B_{eff} .

The fluxes are scaled with respect to the initial conditions in a way that the differences between the plotted curves are due only to differences in mixing behaviour. Therefore the curves coincide at low heights where mixing has not yet had a strong influence. Such a scaling is straight forward since time and area integrated fluxes of a conserved quantity at a given height are identical to the total amount of that quantity that has passed through that level. Accordingly the mass flux in the upper graph has been scaled by the volume* of the initial bubble (i.e. the volume where $\Delta h > 0$). The second graph shows the Δh flux of the updraft which is the Δh flux integrated over the

* Since the average density of the initial bubble is the same for all runs, scaling by the volume is proportional to scaling by the mass of the initial bubble.

area where $\Delta h > 0$. This quantity is scaled by the initial bubble volume times the initial maximum of Δh . The total h flux in the last graph is scaled by the the initial bubble volume times the largest h difference occurring in the system at the initial time, i.e. the highest cloud value minus the environmental value of h .[†] This provides a different scale than the maximum of Δh , which was defined as the difference between the cloud value of h and the saturation value for the environment.

The initial bubble in Fig. 4 is located between $z = -1$ and $z = 1$, since height is scaled with respect to the bubble radius. While the h fluxes (lower graphs) monotonically decrease with height for $z > 1$, the slope of the mass flux curves (upper graph) can have either sign. In a finite region above $z = 1$ the mass flux curves are seen to increase, decrease or to stay roughly constant, depending on the initial value of B_{eff} . This behaviour is consistent with the early-time evolution of the volume of the active cloud (third graph in Fig. 3) which was discussed above in terms of the mixing diagrams (Fig. 1) in section 2.

Probably more surprising than the initial slope above $z = 1$ is the abrupt change in regimes of these curves. While in the first region above $z = 1$ the respective slope of the mass flux curves varies only slowly, the end of this region is marked by a sharp transition to a region where the mass flux decreases more rapidly. The observed change of regimes is also reflected in a similar behaviour of the moist static energy fluxes. Generally the flux curves in Fig. 4 can be roughly divided into three parts with height: (i) The region between $z = -1$ and $z = 1$ where the initial bubble is located, (ii) a region of only slowly varying slope, and (iii) a "collapse region" where the fluxes vanish in a more rapid and generally less regular fashion. For the mass and Δh flux (upper graphs) the slope and the height of the second region appears to be largely determined by the respective value of B_{eff} . This is different for the total h flux, whose slope in this region depends more strongly on the actual buoyancy. For the strong bubbles (ΔT large, or L_{eff} small) the total- h flux decays very little in region (ii). This indicates that, in this region, the strong bubbles drag along most of the initially buoyant air even if it has become nonbuoyant through mixing. A strictly constant 'total h flux' above $z = 1$ would indicate that all the air which is initially buoyant rises to the top, as happens in the absence of reevaporation in which case all the initially buoyant fluid remains buoyant. Finally, of course, the negatively buoyant fluid is left behind, even for the strong updrafts which collapse roughly in the same region as the less buoyant ones with the same B_{eff} . This illustrates that the loss of buoyancy which causes the collapse of the cloud is better represented by the Δh flux shown in the middle graph than by the 'total h flux' which also involves the nonbuoyant air that cannot rise with the updraft for a very long time.

(c) *The influence of the buoyancy length scale*

An interesting difference between moist and dry convection is the stratification of the environment which, as explained above, introduces a length scale $L_{buo} = \Delta T / \Delta \Gamma$. This leads to scale independent parameter $L_{eff} = L / L_{buo}$. In the preceding sections we showed that L_{eff} plays only a secondary role in the evolution of the updraft, which is largely determined by the effective buoyancy B_{eff} . This length scale has, however, quite interesting consequences for the geometry of the updraft which is illustrated in Fig. 5. The figure shows snapshots of Δh (left panels) and potential temperature (right panels),

[†] Determining the total h flux related to the updraft in a strict sense requires extremely long simulation until all the cloud water has been reevaporated and the whole domain is dry and stably stratified. In this article we focus on the convective properties in the more active phase of the cloud. The total h flux in the bottom graph of Fig. 4 therefore is integrated only until a time where this active phase is over, and changes occur on a much slower time scale.

taken at the same nondimensional time for three updrafts with the same B_{eff} and the same physical length (i.e. the same initial radius $L = 720m$) but a different effective length $L_{eff} \propto L/\Delta T$. One finds that the horizontal width of the updraft increases with increasing buoyancy length $L_{buo} = \Delta T/\Delta\Gamma$ and for large L_{buo} the h excess is increasingly focussed in a vortex ring at the edge of the cloud (the cross section of the ring is given by the two Δh maxima). Correspondingly, as L_{buo} decreases, (i.e. L_{eff} increases) the updraft exhibits increasingly finer structures and the moist static energy excess is increasingly more weighted towards the center. The weakest of the three updrafts (top graph) has even developed smaller updrafts at the top (upper bright regions), which separated at an earlier stage from the ringlike structure below.

To understand how L_{buo} influences the structure of the cloud, it is instructive to study the velocity field shown by the vectors in the right panels of Fig. 5. The white lines mark the boundary of the saturated (cloud) air. While for the weak cloud (top) the velocity outside of the saturated area is very small and almost exclusively horizontal, the strong cloud (bottom) has a strong circulation centered near the cloud edge, which powerfully sweeps unsaturated air from below into the cloud. This different behaviour for different ΔT is not surprising since vertical motion outside of the cloud requires work against the stratification. This work is done by the pressure gradient resulting from the ascent of the bubble which must push air away at its top and replace the air at its bottom. Since L_{buo} is the strength ΔT of the updraft divided by the stratification $\Delta\Gamma$, it is related to the vertical height across which the pressure difference built up by the buoyancy can force unsaturated air. This yields an upper limit for the size of the large eddies that cross the cloud boundary and are responsible for the entrainment of environmental air.

The difference in eddy size is also responsible for the different form of the updrafts seen in Fig. 5. For the strong updraft (bottom panels), large entraining eddies have strongly eroded the moist static energy excess in the center and pushed the most buoyant regions further apart. They have also eroded the saturated region more effectively than in the weak bubble for which cloud base remains near the initial bubble height. For the weak cloud (top panel), the eddy size is not sufficient to erode the center, and it remained positively buoyant for a longer time and developed smaller updrafts.

Since each thermal weakens (and finally collapses) during its ascent, L_{buo} decreases continuously throughout the cloud's lifetime. Correspondingly, the initially most buoyant clouds eventually developed finer structures and broke up into increasingly smaller turrets. In contrast to the initially weaker clouds, however, these smaller updrafts tend to be distributed further around the edge of the originally stronger clouds where a core of buoyant air was protected within the vortex ring. For initially stronger updrafts with the same B_{eff} , the environment is dryer, and in these cases the smaller turrets that develop later in the evolution of the cloud collapse sooner.

5. CONCLUSIONS

In this paper we have introduced a simple model for a moist convective thermal. The use of such a model problem was motivated by previous work with laboratory analogues, but rather than be constrained by fluid systems that are available in the laboratory, we have considered a problem that includes both of the principal effects of latent heat, namely its release as the thermal rises and its consumption through reevaporation of cloud water. Release of latent heat implies that, although we consider an atmosphere that is neutrally stratified with respect to the saturated rising air, it is stably stratified in the unsaturated environment. Not surprisingly this dynamics, sometimes referred to

as moist up/dry down, has important consequences for the structure of the cloud, as discussed below.

The current investigation also differs from the classical studies of buoyant thermals in that we did not try to enter the self-similar regime where the dynamics become independent of the initial geometry and size. As discussed in the introduction, such a regime is not generally believed to be of great relevance for real clouds. The question remains whether updrafts exhibit some kind of self-similar structure in the smaller-scale turbulence, which might justify the entrainment hypothesis discussed in the introduction. While quite regular behaviour of the fluxes over a certain range of heights (regime 2 in section 4.b) might be an indicator of some degree of self-similarity at these levels, the current data do not allow the test of a particular self-similarity hypothesis, nor is it clear that such an hypothesis would apply over large enough region to make it useful in the description of clouds.

Our data however reveal an approximate dynamical similarity in that the effect of the mixing process on certain quantities is largely determined by a single scale-independent parameter (which we called the effective buoyancy B_{eff}) and is relatively insensitive to other parameters. This property appears to be quite robust for time series and flux-height plots of mass and moist static energy integrated over the "active cloud" region where $\Delta h > 0$. Interestingly it does not work very well for the total h flux, which is the integral over the whole domain, including negatively buoyant air. This indicates that the transport by air with $\Delta h < 0$ does not exhibit the same degree of dynamic similarity, i.e. it cannot be (approximately) described by B_{eff} alone.

In the presence of buoyancy reversal due to re-evaporation, it is less straight forward to define the boundary of a thermal across which entrainment and detrainment occurs, and different definitions are used in the convection literature. Our results suggest that $\Delta h > 0$ is a useful choice when seeking similarity properties for the mixing behaviour. This definition is particularly convenient for analysing the decay and the final collapse of the updraft as it involves all the "active cloud air" (i.e. the air which remains positively buoyant when lifted to its condensation level).

An interesting result of this work, which appears to be consistent with the experiments of Johari (1992), is that B_{eff} must be much larger than 1 for the bubble to rise significantly more than one diameter. This implies that for a bubble with a realistic buoyancy excess the environment must be extremely moist (almost saturated - see table 3). Isolated buoyant thermals therefore appear to be diluted by entrainment quite vigorously and require an extremely moist environment to remain buoyant for a reasonably long time. The air that reaches cloud top in deep convecting clouds must therefore have risen predominantly into air premoistened by previous updraft air. This may occur in a more continuous fashion (similar to a plume) or in distinct bubbles. Observations suggest that both possibilities occur in nature (Barnes et al. 1996, French et al. 1999).

It is worth noting that $B_{eff} = c_p \Delta T / (L_v q_{def})$ depends only on the water vapour deficit q_{def} , and is independent of the actual water vapour content or the relative humidity. Indeed neither the water vapour mixing ratio nor the saturation value q_{sat} explicitly occur in our model equations (only the z -derivative of q_{sat} and q_{def}). These quantities enter the equations of motion for the real atmosphere only through the virtual temperature effect, which is a second-order effect when compared to the effects of latent heat release.

An important result of this study is that the stratification of the environment $\Delta \Gamma$ introduces a length scale $L_{buo} = \Delta T / \Delta \Gamma$ for an updraft with a buoyancy excess ΔT . The resulting dimensionless parameter $L_{eff} = L / L_{buo}$ for a thermal with radius L has been referred to as effective bubble length in this article. Increasing this effective bubble length

(by decreasing L_{buo} for constant L) we found that the radius of the thermal remained smaller during its ascent. The thermal expanded less in the horizontal and exhibited increasingly finer structures for smaller values of L_{buo} . For sufficiently large L_{eff} the thermal broke up at an early stage of its evolution by developing smaller turrets at its top. Since $L_{eff} \propto L/\Delta T$ decreases as a thermal spreads out and reduces its buoyancy through mixing, every thermal finally broke up into smaller turrets (which however collapsed quite rapidly if the environment was sufficiently dry).

This effect of $L_{eff} = L/L_{buo}$ on the bubble's geometry was explained by relating L_{buo} to the maximal depth of forced downdrafts, which yields an upper limit for the vertical extent of the largest eddies. If L_{eff} is small these eddies are of the size of the thermal. They play a crucial role for mass conservation as they transport fluid from its top to its bottom as the thermal rises. If L_{eff} is large this transport is suppressed and the thermal breaks up in order to rise. This behaviour suggests the existence of a characteristic length scale for the largest eddies involved in entrainment. For typical atmospheric conditions, L_{buo} has a value of a few hundred meters. Since this is not necessarily small in comparison to the size of the cloud, this scale will be difficult to observe. However, forced downdrafts are often seen (Yuter and Houze 1995) and their characteristic scale may help to explain observations that some cumulus clouds appear to develop as a single entity, while others are better described as a series of bubbles.

While L_{eff} seemed to have little effect on the final height reached by a bubble (which was largely determined by B_{eff}), it could still have a significant influence on the net transport and latent heat release. Decreasing L_{eff} led to an enhanced upward transport of negatively buoyant air with the thermal, causing a larger moist static energy flux. For understanding this enhanced lifting of negatively buoyant air an alternative (but equivalent) interpretation for L_{eff} may be useful. One has $L_{eff} = [T_{buo}/T_{BV}]^2$ where T_{BV} is the Brunt-Väisälä time scale on which the stratification of the environment is restored. Thus small L_{eff} indicates that the bubble perturbs the buoyancy on a time scale too fast for the restoring forces to counter it, while large L_{eff} means that the bubble's motion is strongly constrained by the stratification.

In this initial investigation of the model we concentrated on two aspects: the effect which the dryness of the environment has on the thermal's mass and energy budgets (which is largely determined by B_{eff}) and secondly the consequences which the stratification has for the thermal's geometry (as governed by L_{eff}). We did not consider the effects of the cloud water content, and the threshold value ql_{max} was kept constant (at $0.75g/kg$) for all the data presented here. Preliminary studies with increased values of ql_{max} indicated that the mixing is slightly increased in these cases (though B_{eff} remains the dominant parameter). Simulations with $ql_{max} = 0$ were still found to exhibit the breakup of the bubble (which confirms that this phenomenon is indeed related to L_{buo} as the downdraft length is zero in this case). A more comprehensive understanding of the role of the cloud water content however will require further study.

For the simple model problem posed here, it has been possible to identify the dominant physical process controlling entrainment. This identification was made by observing an approximate dynamical similarity where a single parameter, B_{eff} , largely controlled the behaviour of the system. It remains to be seen whether the process measured by B_{eff} , i.e. the loss of buoyancy of cloud air due to mixing with unsaturated environmental air, also controls entrainment in real clouds, but at a minimum this provides an hypothesis to be tested in future studies with observations and more realistic models. The existence of an approximate dynamical similarity in no way implies that the self-similarity of the dry thermal is present in the moist problem studied here. Indeed, both of the controlling

nondimensional parameters, B_{eff} and L_{eff} , depend on properties of the initial bubble. Similarly, it may be expected that the behaviour of real clouds will be strongly influenced by the properties of the boundary layer air at the time of initiation. At present, little is known: it is virtually impossible to make observations at the precise location where a cloud is about to form, while modelling studies must specify initial conditions of some sort.

ACKNOWLEDGEMENT

This work was supported by the UK Meteorological Office. We would like to thank Mike Gray and Andy Brown for providing and supporting us in the use of the latest version of the large eddy simulation (LES) model of the UK Meteorological Office. In particular, Mike Gray is thanked for providing us with the stretched grid update. Adrian Tompkins is thanked for valuable assistance with LES model and interesting discussions.

APPENDIX

Numerical Details

The simulations were performed using the numerical model described by Shutts and Gray (1994), which is based on the Arakawa C-grid, and uses the total variation diminishing advection scheme of Leonard (1991), which is less diffusive than most comparable schemes. The domain was square with $(72 \times 72 \times 150)$ grid points, corresponding to a physical size of $(40\text{km} \times 40\text{km} \times 12.25\text{km})$. The vertical resolution was constant ($DZ = 75\text{meters}$) and stretched coordinate system was used in the horizontal directions with a square central region of size 3.6 km and 75 meter resolution. Beyond that region the grid spacing increased approximately exponentially with the distance from the center. Initially this increase was very slow, leading roughly to a doubling of DX over the first kilometer. After this we used a larger exponent fitted to the overall domain size of 40km. This large domain was used to ensure that subsidence would not significantly alter the environmental sounding. (A visual impression of the model's resolution near the center may be obtained from Fig. 5 where velocity vectors are given at every second horizontal and vertical grid point.)

The horizontal boundary conditions were periodic while zero flux (insulating) boundaries were applied at the top and bottom of the domain. A Newtonian damping layer was employed over the upper kilometer at the domain top in order to damp gravity waves.

The initial bubble had its center 3 km above the surface, which was found to be sufficient to make results independent of the lower surface. Tests were also carried out to ensure that the particular choice of the stretched grid did not significantly influence the results.

Figure Captions:

- Figure 1 Mixing diagrams for moist static energy excess Δh (grey solid line) and liquid water static energy excess Δh_l (dotted line) as function of the fraction of entrained environmental air α . In figures Ia) and Ib) the dark solid line indicates $c_p \Delta T$ (a more direct measure for buoyancy). In figure II) the dark solid line is proportional to the downdraft length L_{down} .
- Figure 2 Snapshots of Δh (left panels) and cloud water (right panels) for different times given above each panel (t in units of T_{buo} see text). At the top left of each Δh plot "max" indicates the maximum of $\Delta h/c_p$ [units: K] (corresponding to the brightest shading of the respective graph). The brightest shading for all cloud-water plots corresponds to $ql_{max} = 0.75g/kg$.
- Figure 3 Time series from experiments with different values of B_{eff} and L_{eff} for (from top to bottom) a) w_{max} : maximal vertical velocity, b) T_{max} : maximal value of ΔT of the region where $\Delta h > 0$, c) integrated mass of air with $\Delta h > 0$ and d) Δh (weighted by density) integrated over the volume with $\Delta h > 0$. All data are scaled in the units discussed in section 3.
- Figure 4 Vertical fluxes integrated over time and horizontal area as a function of height for the experiments with different values of B_{eff} and L_{eff} as in Fig. 3. From top to bottom a) mass flux integrated over the region where $\Delta h > 0$, b) Δh flux integrated over the region where $\Delta h > 0$, c) h flux integrated over the entire domain. All fluxes are scaled as described in the text.
- Figure 5 Snapshots at $t = 9.4T_{buo}$ for experiments with $B_{eff} = 3.15$ and different values of L_{eff} (30 top, 7.5, middle, 0.83, bottom). Plotted are Δh (left) and potential temperature (right). White contours mark the boundary between saturated and unsaturated air. Vectors indicate the velocity field. The cross sections are taken approximately 400 meters away from the thermal's center where the weakest of the plotted thermals (top panels) has developed two smaller turrets at its top.

REFERENCES

- | | | |
|--|------|---|
| Arakawa, A and Schubert, W. H. | 1974 | Interaction of a cumulus cloud ensemble with the large scale environment. <i>J. Atmos. Sci.</i> , 31 , 674-701 |
| Baker, B. A. | 1992 | Turbulent entrainment and mixing in clouds: a new observational approach. <i>J. Atmos. Sci.</i> , 49 , 387-404 |
| Baker, M. B. and Breidenthal, R. E. | 1984 | The effects of turbulent mixing in clouds. <i>J. Atmos. Sci.</i> , 41 , 299-304 |
| Barnes, G. M., Frankhauser, J. C. and Browning, W. D. | 1996 | Evolution of the vertical mass flux and diagnosed net lateral mixing in isolated convective clouds <i>Mon. Wea. Rev.</i> , 124 , 2764-2784 |
| Blyth, A. M. | 1993 | Entrainment in cumulus clouds. <i>J. Appl. Meteor.</i> , 32 , 626-641 |
| Bretherton, C. S. | 1997 | Entrainment, detrainment and mixing in atmospheric convection. <i>The physics and parametrisation of moist atmospheric convection</i> editor Smith, R. K., Kluwer Academic Publishers 211-230 |
| Carpenter JR., R. L., Droegemeir, K. K. and Blyth, A. M. | 1998 | Entrainment and detrainment in numerically simulated cumulus congestus clouds. Part I: General results. <i>J. Atmos. Sci.</i> , 55 , 3417-3432 |
| French, J. R., Vali, G. and Kelly, R. D. | 1999 | Evolution of small cumulus clouds in Florida: observations of pulsating growth. <i>Atmos. Res.</i> , 52 , 143-165 |
| Grabowski, W. W. | 1993 | Cumulus entrainment, fine-scale mixing and buoyancy reversal. <i>Q. J. R. Meteorol. Soc.</i> , 119 , 935-956 |
| | 1995 | Entrainment and mixing in buoyancy reversing convection with application to cloud-top entrainment instability. <i>Q. J. R. Meteorol. Soc.</i> , 121 , 231-254 |

- Johari, H. 1992 Mixing in thermals with and without buoyancy reversal. *J. Atmos. Sci.*, **49**, 1412-1426
- Kain, J. S. and Fritsch, J. M. 1990 A one-dimensional entraining-detraining plume model and its application in convective parametrisation. *J. Atmos. Sci.*, **47**, 2784-2802
- Kitchen, M. and Caughey, S. J. 1981 Tethered-balloon observations of the structure of small cumulus clouds. *Q. J. R. Meteorol. Soc.*, **107**, 853-874
- Klaassen, G. P. and Clark, T. L. 1985 Dynamics of the cloud-environment interface and entrainment in small cumuli: Two-dimensional simulations in the absence of ambient shear. *J. Atmos. Sci.*, **42**, 2621-2642
- Leonard, B. P. 1991 The ULTIMATE conservative difference scheme applied to unsteady one-dimensional advection. *Comput. Methods Appl. Mech. Eng.*, **88**, 17-74
- Lesieur, M. 1997 *Turbulence in fluids*, third edition, Kluwer Academic Publishers
- Ludlam, F. H. and Scorer, R. S. 1953 Convection in the atmosphere. *Q. J. R. Meteorol. Soc.*, **79**, 94-103
- Malkus, J. S. and Scorer, R. S. 1955 The erosion of cumulus towers. *J. Meteorol.*, **12**, 43-57
- Mason, P. J. 1994 Large-eddy simulation: A critical review of the technique. *Q. J. R. Meteorol. Soc.*, **120**, 1-26
- Morton, B. R. 1997 *The physics and parametrisation of moist atmospheric convection* editor Smith, R. K., Kluwer Academic Publishers 143-175
- Morton, B. R., Taylor, G. I. and Turner, J. S. 1956 Turbulent gravitational convection from maintained and instantaneous sources. *Proc. Roy. Met. Soc. London*, **A234**, 1-23
- Sánchez, O., Raymond, D. J., Libersky, L and Petschek, A. G. 1989 The development of thermals from rest. *J. Atmos. Sci.*, **46**, 2280-2292
- Shutts, G. J. and Gray, M. E. B. 1994 A numerical modelling study of the geostrophic adjustment process following deep convection. *Q. J. R. Meteorol. Soc.*, **120**, 1145-1178
- Smith, S. A. and Jonas, P. R. 1995 Observations of the turbulent fluxes in fields of cumulus clouds. *Q. J. R. Meteorol. Soc.*, **121**, 1185-1208
- Squires, P. and Turner, J. S. 1962 An entraining jet model for cumulonimbus updrafts. *Tellus*, **14**, 422-434
- Tiedtke, M. 1989 A comprehensive mass flux scheme for cumulus parametrisation in large scale models. *Mo. Wea. Rev.*, **117**, 1779-1800
- Turner, J. S. 1973 *Buoyancy effects in fluids*, Cambridge University Press
- 1986 Turbulent entrainment: The development of the entrainment assumption and its application to geophysical flows. *J. Fluid. Mech.*, **173**, 431-471
- Turner, J. S. and Yang, I. K. 1963 Turbulent entrainment at the top of stratocumulus clouds. *J. Fluid. Mech.*, **17**, 212-224
- Venkatakrisnan, L, Bhat, G. S. and Narasimha, R. 1999 Experiments on a plume with off-source heating. *J. Geophys. Res.*, **104**, 14271-14281
- Warner, J. 1970 On steady-state one-dimensional models of cumulus convection. *J. Atmos. Sci.*, **27**, 1035-1040
- Yuter, S. E. and Houze, R. A. 1995 Three-dimensional kinematic and microphysical evolution of florida cumulonimbus. Part II: Frequency distributions of vertical velocity, reflectivity and differential reflectivity. *J. Atmos. Sci.*, **123**, 1941-1963

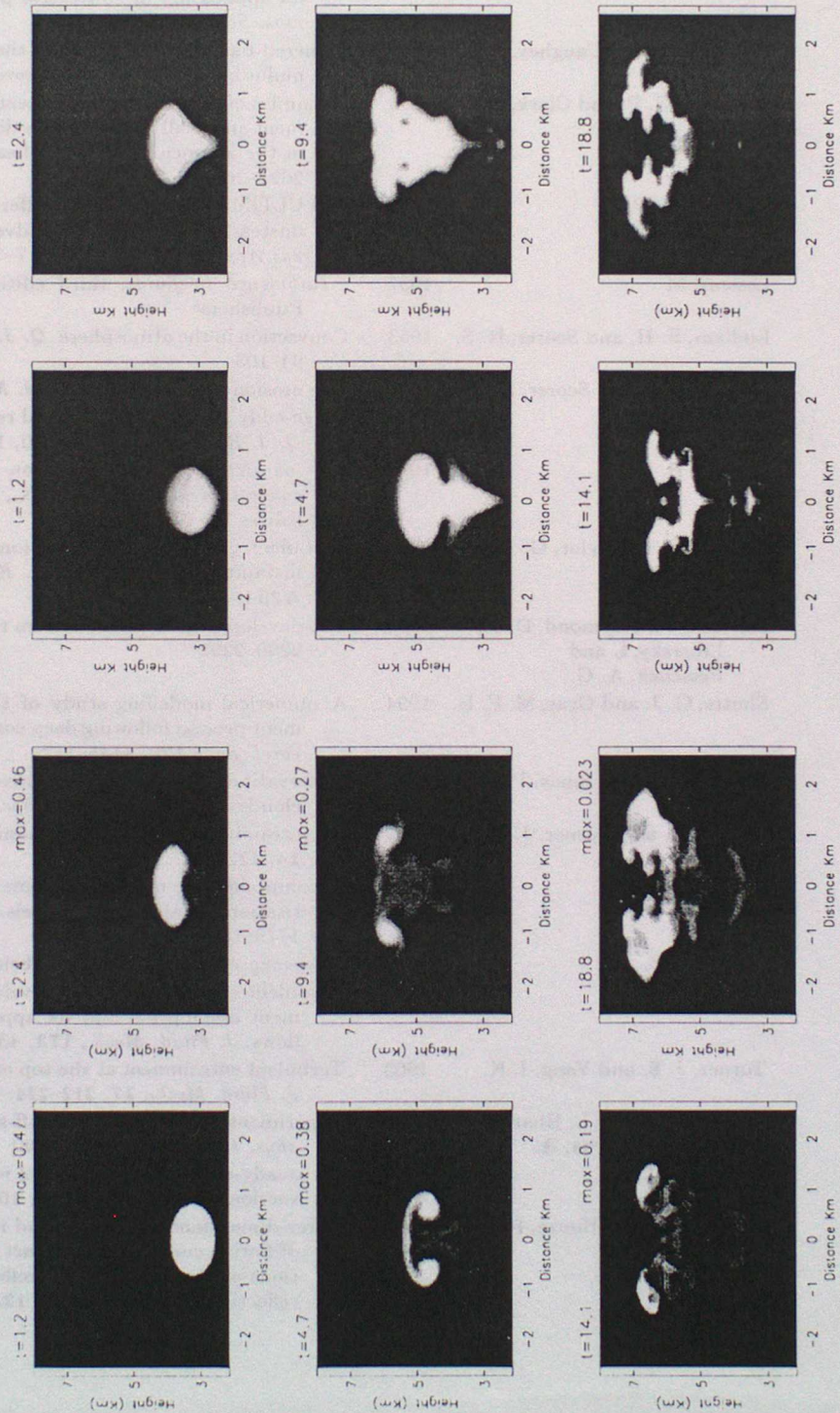


Figure 2. Snapshots of Δh (left panels) and cloud water (right panels) for different times given above each panel (t in units of T_{bu0} see text). At the top left of each Δh plot "max" indicates the maximum of $\Delta h/c_p$ [units: K] (corresponding to the brightest shading of the respective graph). The brightest shading for all cloud-water plots corresponds to $q_{l,max} = 0.75g/kg$.

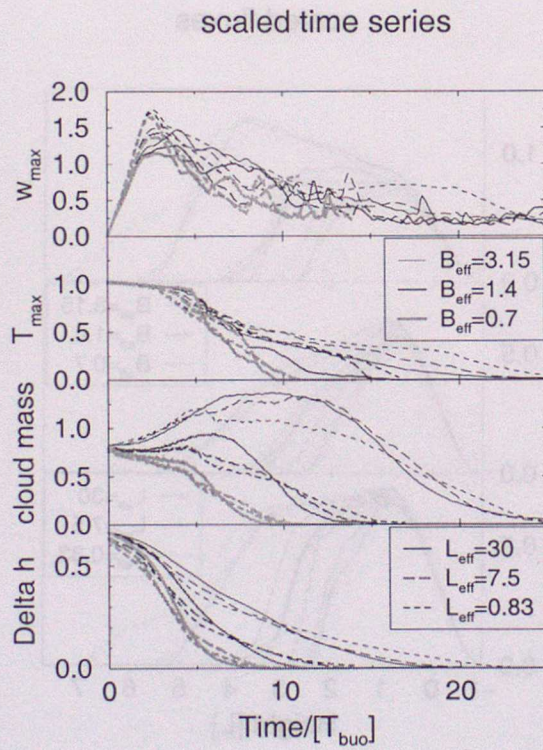


Figure 3. Time series from experiments with different values of B_{eff} and L_{eff} for (from top to bottom) a) w_{max} : maximal vertical velocity, b) T_{max} : maximal value of ΔT of the region where $\Delta h > 0$, c) integrated mass of air with $\Delta h > 0$ and d) Δh (weighted by density) integrated over the volume with $\Delta h > 0$. All data are scaled in the units discussed in section 3.

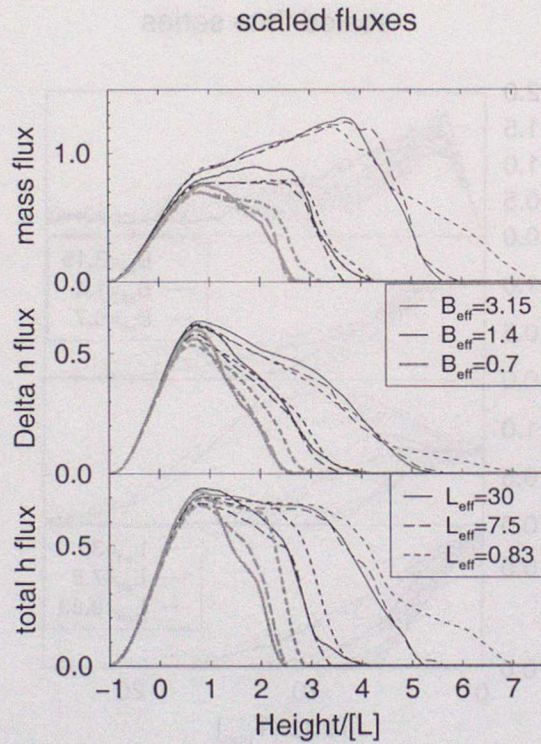


Figure 4. Vertical fluxes integrated over time and horizontal area as a function of height for the experiments with different values of B_{eff} and L_{eff} as in Fig. 3. From top to bottom a) mass flux integrated over the region where $\Delta h > 0$, b) Δh flux integrated over the region where $\Delta h > 0$, c) h flux integrated over the entire domain. All fluxes are scaled as described in the text.

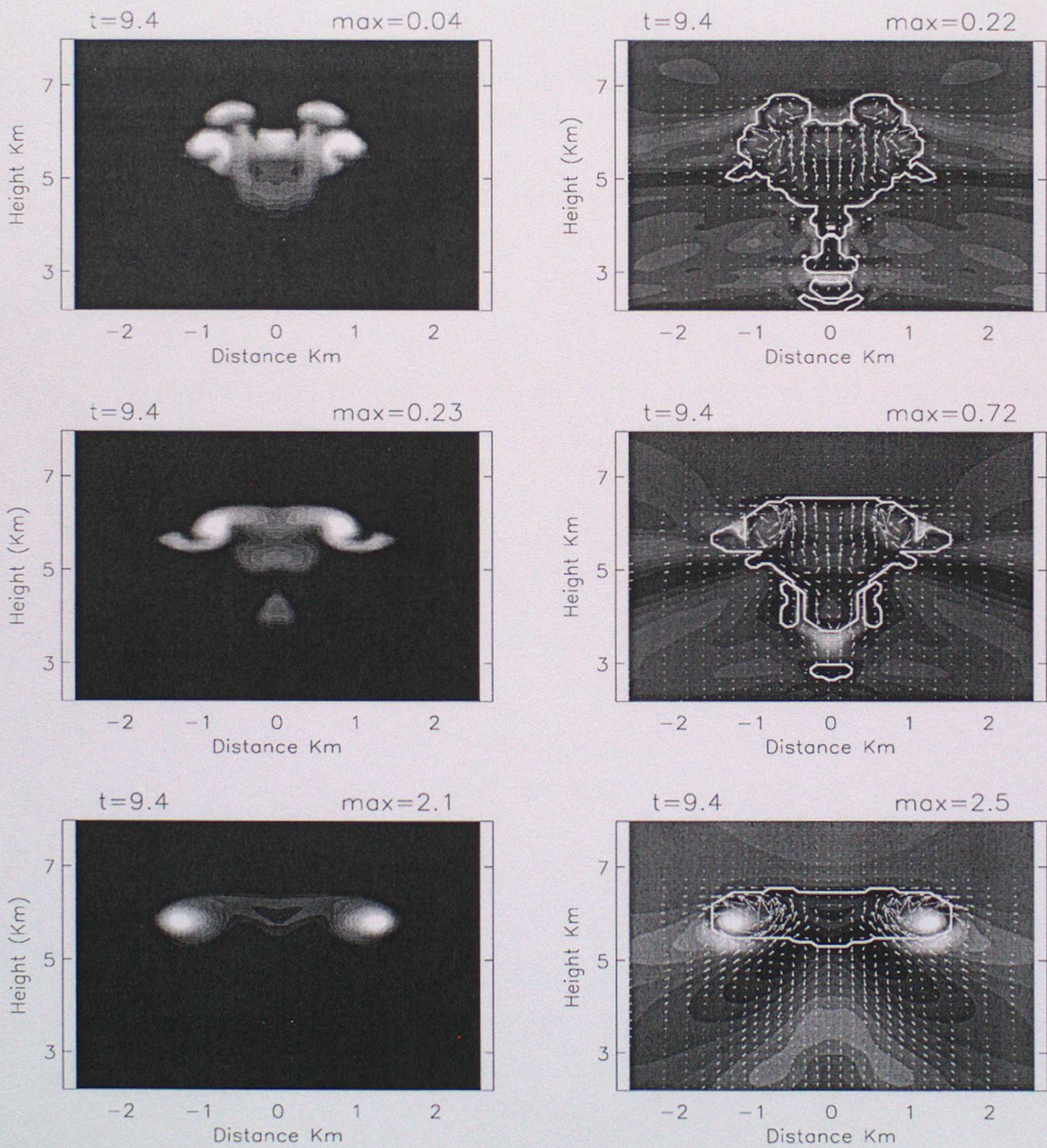


Figure 5. Snapshots at $t = 9.4T_{buo}$ for experiments with $B_{eff} = 3.15$ and different values of L_{eff} (30 top, 7.5, middle, 0.83, bottom). Plotted are Δh (left) and potential temperature (right). White contours mark the boundary between saturated and unsaturated air. Vectors indicate the velocity field. The cross sections are taken approximately 400 meters away from the thermal's center where the weakest of the plotted thermals (top panels) has developed two smaller turrets at its top.